Fabrication of succinate-alginate xerogel films for in vitro coupling of osteogenesis and neovascularization

Joseph Deering[1], Dawn S. Y. Lin[2], Andrew D'Elia[1], Boyang Zhang[2,3], Kathryn Grandfield[1,3,4*]

[1] Department of Materials Science and Engineering, McMaster University, Hamilton, ON, Canada

[2] Department of Chemical Engineering, McMaster University, Hamilton, ON, Canada

[3] School of Biomedical Engineering, McMaster University, Hamilton, ON, Canada

[4] Brockhouse Institute for Materials Research, McMaster University, Hamilton, ON, Canada

[*] Corresponding author:
Prof. Kathryn Grandfield
McMaster University
1280 Main Street West
Hamilton, ON, L8S 4L7
Canada
Email: kgrandfield@mcmaster.ca

Abstract

The osseointegration of metallic implants is reliant on a cascade of molecular interactions and the delivery of macromolecules to the implant environment that occurs before substantial bone formation. Early blood vessel formation is a requisite first step in the healing timeline for osteoid formation, where vascular development can be accelerated as a result of controlled hypoxic conditioning. In this study, alginate-derived xerogel films containing varied concentrations of disodium succinate salt which has been shown to induce pseudohypoxia (short-term hypoxic effects while maintaining an oxygenated environment) were developed. Xerogels were characterized for their morphology, succinate release over time and cellular response with osteoblast-mimicking Saos-2 and human umbilical vein endothelial cells (HUVEC). Scanning electron microscopy revealed a multiscale topography that may favour osseointegration and alamarBlue assays indicated no cytotoxic effects during *in vitro* proliferation of Saos-2 cells. pH measurements of eluted succinate reach 95% of peak value after 7 hr of immersion for all gels containing 10 mM of succinate or less, and 60% within the first 40 min. *In vitro* exposure of HUVECs to succinate-conditioned media increased the net concentration of total proteins measured by bicinchoninic acid (BCA) assay and maintains stable vascular endothelial growth factor (VEGF) and extracellular platelet-derived growth factor (PDGF) for vessel formation through comparison of enzyme-linked immunosorbent assays (ELISAs) of the culture media and cell lysate. Tube formation assays also showed a sustained increase in tube diameter across the first 48 hr of HUVEC culture when succinate concentrations of 1 and 10 μM in the xerogel. Overall, the succinate-alginate films serve as a prospective organic coating for bone-interfacing implant materials which may induce temporary pseudohypoxic conditions favourable for early angiogenesis and bone regeneration *in vivo* at succinate concentrations of 1 or 10 μM.

Keywords

Pseudohypoxia; Implant coating; Neovascularization; Succinate; Xerogel; Bone Regeneration

1 Introduction

At the core of total joint replacement and dental procedures, success is contingent on the integration of implant materials with existing bone and connective tissue in a process termed 'osseointegration' [1]. Failure of classical implants has sparked the development of biomaterials and bioactive agents that mimic and support the growth of bone tissue while addressing root causes of implant failure, especially where improvement in short-term bone ingrowth and direct bone-implant contact has been correlated to long-term implant success [2]. Coating deposition offers a means to improve the bioactivity of the native implant surface and techniques including electrodeposition [3,4], dip coating [5,6], plasma spraying [7,8], or vapor deposition [9,10] are available to apply organic, ceramic, or composite films to a metallic prosthesis. In particular, immersion-based strategies can be better than line-of-sight techniques for coating the entirety of materials with complex or porous geometries. Matrix materials such as chitosan [11,12], alginate [13,14], and hyaluronic acid [15,16] exhibit the capacity to deliver biomolecules directly to the bone-implant interface while simultaneously mimicking the structure of the natural extracellular matrix in hydrogel form [17]. Integration of nanoceramics, therapeutic drugs and growth factors, and/or antimicrobial agents into these gel-based coatings may improve long-term outcomes of the implant. However, the early osteoinductive pathway begins long before any form of bone mineral apposition with the formation of a blood vessel network.

Neovascularization within the surgically resected volume is one step within the osteoinduction process, where the development of new blood vessels is pivotal for driving local cell recruitment and potentiating macromolecular transport [18]. Aside from facilitating waste transport and oxygen delivery, the formation of new blood vessels allows for direct migration of osteogenic progenitor cells and relevant growth factors [19], where angiogenic growth factors such as vascular endothelial growth factor (VEGF) or platelet-derived growth factor (PDGF) can serve as osteoblastic and osteoclastic chemoattractants on the surface of implant materials [20,21]. The exogenous addition of these compounds has resulted in favourable vascular development in general tissue engineering [22] and cardiac-specific [23] applications. Tumour angiogenesis can also be attributed to these factors [24]. Elution of angiogenic growth factors in the peri-implant environment has been shown to increase proliferation and differentiation of cells during the development and remodeling of blood vessels in a generalized manner [25–27]. Specifically, the presence of VEGF influences cell fates in a complex, time-dependent manner. Early in the angiogenic cascade, VEGF can encourage survival of cells with an endothelial origin [28] but prolonged exposure can cause leakage in more mature vascular networks [29]. Angiogenic agents have been incorporated into materials in various studies to facilitate formation of new blood vessels both *in vivo* and *in vitro* [30–34], but the recombinant form of growth factors can be sensitive to handling/storage [35] and their efficacy depends highly on structural preservation of subunits [36] making them difficult agents to incorporate into biomaterial coatings.

The family of hypoxia-related genes, which are stimulated in oxygen-starved environments, is regulated by transcription factor hypoxia-inducible factor 1-alpha (HIF-1α) [37]. Upstream stabilization of HIF-1α has been shown to have direct consequences on activating hypoxia responsive elements (HREs) in the nucleus and can result in further endogenous upregulation of angiogenic growth factors (PDGF and VEGF) and angiogenesis as a whole [38]. Within normoxic environments (Figure 1i), existing HIF-1α within the cellular domain is tagged with a hydroxyl group by prolyl hydroxylase 2 [39] and HIF-1α is subsequently subjected to proteasomal degradation after its ubiquitination with von Hippel Lindau [40]. In hypoxic environments (Figure 1ii), the

absence of oxygen allows the HIF-1α complex to bypass the hydroxylation step of the typical degradation process and translate to activate nuclear HREs, resulting in increased levels of angiogenic proteins [41]. Extending to an *in vivo* setting, prolonged hypoxia and ischemia can have more far-reaching negative consequences. In bone especially, ischemic mechanisms are commonly the final stage in avascular necrosis of the tissue [42]. However, it is possible to alter the HIF-1α pathway without disrupting oxygen levels in the tissue. The stabilization of HIF-1α with precise administration of cobalt chloride is something that has been recently investigated for angiogenic applications and has resulted in upregulation of VEGF and activation of vascular cell progenitors [43–45], although its long-term health effects are still being observed. Due to its potentially hazardous nature [46], it is important to establish viable alternatives for controlled coupling of angiogenesis and osteogenesis at the implant surface. Succinate, a naturally-derived metabolite, offers the capability to produce a similar pseudohypoxic response (Figure 1iii) within the cell where it serves as both a competitive inhibitor and product of prolyl hydroxylases [47]. In theory, tuning the local release profile of succinate within the implant environment can temporarily control how much HIF-1α bypasses the hydroxylation stage and translocates to activate HREs.

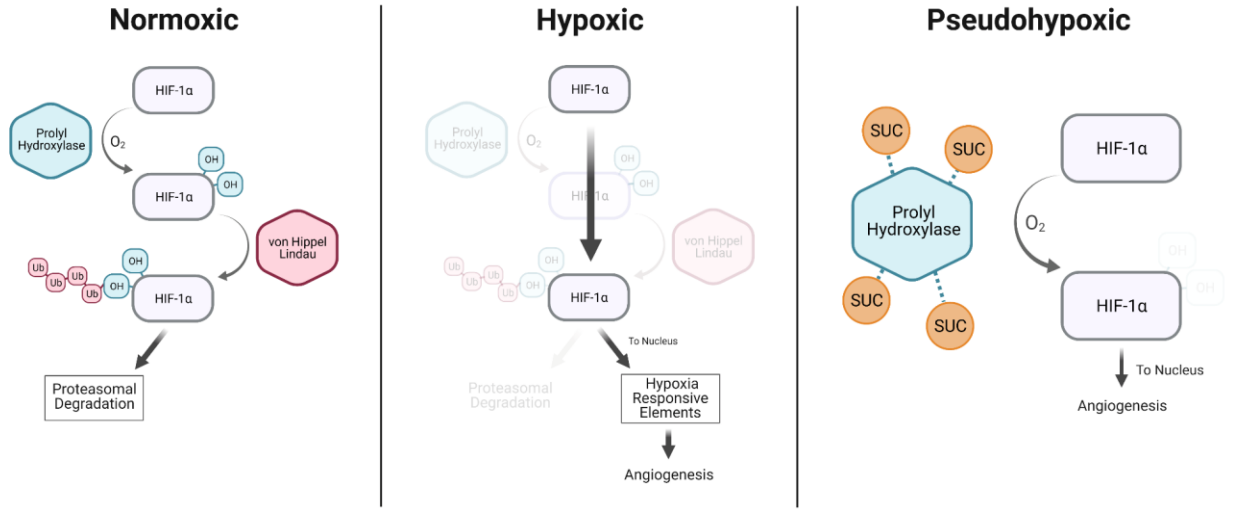

Figure 1: *Pathways for HIF-1α under: (i) Normoxic conditions, where prolyl hydroxylase tags HIF-1α with a hydroxyl group for subsequent ubiquitination, and there is no corresponding activation of hypoxia responsive elements. (ii) Hypoxic conditions, where the absence of oxygen allows high amounts of stable HIF-1α to be translated to the nucleus and upregulate the production of angiogenic factors. (iii) Pseudohypoxic conditions, where the addition of succinate serves as a competitive inhibitor for prolyl hydroxylase and partial translation of HIF-1α to the nucleus occurs as a result.*

In this work, we assess the viability and *in vitro* response of alginate-encapsulated succinate as a coating material for implants. By isolating cell studies to assess osteocompatibility and endothelial activity, we aim to characterize the *in vitro* influence of succinate-stabilized HIF-1α as a tool for fabricating tunable implant surfaces and implicate corresponding responses for bone mineral apposition rates.

2 Methods

2.1 Xerogel synthesis

Stock solution of 3 wt% alginic acid sodium salt (1.56 mannuronate-to-guluronate ratio, MilliporeSigma) in deionized water was prepared by mixing at 800 RPM for 20 min until a notable viscosity change was observed and the solution appeared homogenous in nature. For each following experimental protocol, the corresponding mass of succinic acid disodium salt (162.05 g/mol, MilliporeSigma) was added to aliquots of the alginate stock solution to produce solutions with succinate concentrations of 100 mM, 10 mM, 1 mM, 100 μM, 10 μM, and 1 μM, pipetting up and down at least fifteen times to mix thoroughly. Xerogels were formed by solvent casting the mixture onto the substrate and drying in air at room temperature for 48-72 hr.

2.2 Scanning electron microscopy

Alginate-succinate coatings were cast directly onto aluminum stubs wrapped in aluminum tape to form a bowl shape for containment (300 μL of casting solution for each 12.7 mm diameter stub). Substrates were left to dry in air for 48 hr prior to imaging. Xerogels were imaged without sputter coating at an accelerating voltage of 5 kV with a JSM-6610LV microscope (JEOL). Gels were rehydrated with 100 μL of 4 vol% choline lactate (2-hydroxyethyl-trimethylammonium L-(+)-lactate, SigmaMillipore) in deionized water to add conductivity to the gels in addition to maintaining hydration under microscope vacuum. Imaging of the hydrated gels was performed at an accelerating voltage of 20 kV.

Characterization of xerogel thickness was conducted by depositing alginate films onto stainless steel substrates using volumes of 2, 3, 4, and 5 μL of alginate per square millimeter. Cross-sections were taken for each substrate and mounted for scanning electron microscopy (JEOL 6610LV, 5 kV), with grayscale-based segmentation of the alginate cross-section performed in Dragonfly 2022.1 and coating thickness measured using a volume thickness map across a span of at least 100 μm.

2.3 Succinate release profiles and surface behaviour

2 mL of each alginate-succinate solution (100, 10, 1, 0.1, 0.01, and 0.001 mM succinic acid disodium salt) was cast into 20 mL borosilicate scintillation vials and allowed to dry completely in air (typically 7 days). 18 mL of deionized water was added to the vials and pH measurements were recorded at 5 min intervals over a span of 36 hours using a pH of 7.00 as a starting point. As succinic acid is classified as a weak acid, the complementary sodium salt produces a minor pH increase upon solubilization. Two replicates were run for release studies in each succinate concentration and the average profile was reported.

The swelling ratio of xerogels at each succinate concentration were also measured. Xerogels were formed by solvent casting 19.1 mL of each alginate-succinate ratio into a 90 mm petri dish and drying for at least 72 hr before cutting into four specimens. The mass of xerogel (roughly 100 mg) was recorded before pipetting excess deionized water (4 mL) on top of the gel to rehydrate over a span of 60 min. After 60 min, rehydrated gels were gently blotted with a laboratory wipe and weighed again to measure their mass gain. Swelling ratios are reported as a percentage mass gain between the rehydrated gels and dry xerogels, using four replicates for each case.

To further validate the presence of disodium succinate within the xerogels, Fourier-transform infrared spectroscopy (FTIR) was conducted on xerogels with succinate concentrations between 1 μM and 100 mM. Specimens were examined by measuring transmittance at a resolution of 4 cm^{-1} using Hyperion 3000 instrumentation (Bruker).

2.4 In vitro osteoblast culture

1 mL of each alginate-succinate gel (100, 10, 1, 0.1, 0.01, 0.001, and 0 mM succinate) was pipetted into individual wells of a 24-well tissue culture polystyrene plate, with six replicates for each test condition, and left to dry for 48 hr. Saos-2 (HTB-85, ATCC) osteoblast-mimicking cells were seeded onto each gel and uncoated wells at a density of 10,000 cells/cm^2 in McCoy's modified 5A media supplemented with fetal bovine serum (13%) and penicillin-streptomycin (1%) as described elsewhere [48]. Plates were incubated at 37°C and 5% CO_2 for metabolic measurement at 1 and 4 days. At these time points, metabolic activity was assessed by incubating in a 5% mixture of alamarBlue™ dye (Life Technologies Inc.) in culture media for 60 min and corresponding fluorescence readings at an excitation-emission wavelength of 540-580 nm. Following the 1-day measurements, culture media was restored to the wells and the same culture was assessed at the 4-day endpoint.

Separate Saos-2 cultures were conducted on succinate-alginate xerogels to measure the production of alkaline phosphatase (ALP) as a marker of matrix mineralization after 1 and 4 days of culture. Cells were grown according to the aforementioned procedure (using 6 replicates per succinate concentration) and lysed using a solution of 0.1% Triton X-100 in phosphate buffered saline. 50 μL of lysate solution was combined with 100 μL of ALP assay buffer (Abcam) and incubated for 20 min before measuring absorbance at 405 nm. Two replicates were extracted from each well.

2.5 In vitro endothelial culture

Green Fluorescent Protein-tagged Human Umbilical Vein Endothelial Cells (GFP-HUVECs, Angio-Proteomie) were cultured in a 0.2% w/v gelatin (Sigma Aldrich) coated flask with Endothelial Cell Growth Media (ECGM2, PromoCell), enriching the media with the relevant concentrations (10^{-4} M to 10^{-6} M) of disodium succinate. To observe vascularization at the implant interface, a 96-well plate was filled with 30 μL of growth-factor reduced Matrigel (Corning) into each well. Immediately after adding Matrigel, the plate was incubated at 37°C and 5% CO_2 for 30 minutes to allow gelation. After gelation, 200 μL of the cell suspension (30,000 cells/cm^2 for ELISAs and 10,000 cells/cm^2 for other analyses) was added on top of the Matrigel in each well. Vascularization was imaged using an image cytometer (BioTek Instruments Inc.) based on a single field of view from each of the four replicates.

Bright-field images were processed in Dragonfly 2020.1 (Object Research Systems) by application of a Sobel filter for edge detection of the tube network and a high-pass grayscale filter for segmentation of the vascular network. Thickness maps were generated from the segmentation for each biological replicate and timepoint in Dragonfly. Maps were overlaid onto the Sobel-filtered images for visualization and raw data exported for quantitative measurements of the tube network. Branching behaviour was operationalized by creating a skeletonization of the tube network in Dragonfly, examining the total number of branching locations, and normalizing with respect to other culture conditions.

After 48 hr of culture and succinate exposure, endothelial cells were lysed with 250 μL of 0.1% Triton X-100 in phosphate-buffered saline for 10 min to permeabilize the cell membrane and

release intracellular proteins. 25 μL of lysis solution from each of the four wells were mixed with 200 μL of bicinchoninic acid reagent and incubated for 30 min, using three replicates for each. Absorbance readings were measured at an incident wavelength of 562 nm and converted to total protein content via a standard calibration curve generated from known concentrations of bovine serum albumin.

HUVEC cells were cultured at a density of 3×10^5 cells/cm^2 in endothelial growth medium-2 with 100 μM, 10 μM, and 1 μM of added disodium succinic acid salt for VEGF-A and PDGF-BB enzyme-linked immunosorbent assays. Cultures were conducted with four replicates and two samples were extracted from each for ELISAs. ELISAs were conducted according to manufacturer instructions using 20 μL of culture media for intracellular PDGF-BB determination, 20 μL of lysate solution for extracellular PDGF-BB determination, 50 μL of culture media for intracellular VEGF-A determination, and 50 μL of lysate solution for extracellular VEGF-A measurement. Absorbance measurements were converted to concentrations using standard calibration curves.

2.6 Statistics

Two-way analyses of variance (ANOVAs) with Tukey's honest significance difference test were used to compare groups of varying succinate concentration in measurements of Saos-2 metabolic rate (n = 6), alkaline phosphatase production (n = 6), HUVEC PDGF-BB content (n = 4), and HUVEC VEGF-A content. One-way analyses of variance were used to observe the effect of time on HUVEC tube thickness within each group and HUVEC total protein content in the BCA assay. All data was processed in R 3.6.1 with significance defined as $p < 0.05$. Error bars in all figures correspond to ± standard deviations.

3 Results and discussion

3.1 Scanning electron microscopy

Solvent cast alginate films deposited in the range of 2-5 μL/mm^2 were able to achieve stable films on the small stainless steel substrates. Above 5 μL/mm^2, partial delamination of the alginate began to occur. Below 2 μL/mm^2, it becomes difficult to completely cover substrates using solvent casting due to the effects of surface tension in the solution. In general, the thickness of alginate xerogels appears to have some dependency on the volume of alginate initially deposited on the substrate (Figure 2), where thicker films are generally observed with a larger starting volume of 3 wt% alginic acid sodium salt solution.

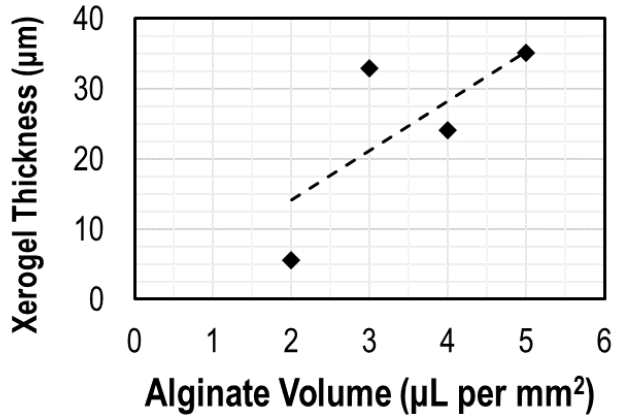

Figure 2: *Alginate xerogel thickness measurements on stainless steel substrates using scanning electron microscopy of the cross-section. Solvent casting with larger volumes of alginate stock solution generally produces thicker xerogels.*

Dehydrated alginate films with and without exogenous succinate addition were then solvent cast to assess their morphology using secondary electron imaging in the scanning electron microscope (SEM). In Figure 3A, the dehydrated film of alginate alone shows a layered, fibre-like structure on the surface of the organic coating, with a series of nanoscale wrinkles that propagate across the entirety of the surface. The optimal surface for osseointegration is described to contain dual-scale topography with both microscale and nanoscale features aiding in the recruitment of osteoblasts and osteoblast progenitors [49], consistent with the topography shown in the dehydrated alginate gels. The wrinkled nature of the alginate xerogel is similar to what has been seen before from dehydrated forms of alginate [50] or other xerogels [51], which appear to contain a continuous network of fibres at their exterior and fulfil the intermediate length scale between nano- and microscale topographies. In the xerogel form, the alginate coatings appear to have a cobblestone-like appearance with consistent long-order patterning (Figure 3A) and a fragmented morphology with intermittent cavities at slightly higher magnification (Figure 3B). Additions of succinate across the millimolar and micromolar range (Figure 3C-H) to the gel casting solution retain this level of multiscale topography, with similar spacing between filaments in the fibrous backbone and similar size of 'fragments' in the xerogel. In all of the alginate-based xerogels, there appears to be circular-appearing regions or striations that are consistent with shrinkage cavities. In both cases, the xerogels consist of concentric fragments and this topography could be attributed to regions of stepwise solidification within the alginate gel. In the case of the 1 mM succinate xerogels, the appearance of striations in place of circular motifs is possibly associated with solvent evaporation behaviour during the drying phase. Concentrations above and below 1 mM both show concentrically-oriented topographies, indicating that either can occur based on drying conditions. Additions of succinate do not appear to significantly alter the homogeneity of the xerogel, and the lack of visible succinate aggregates indicates relatively uniform dispersion throughout the coating material.

Inducing vascular development at an implant site has also been shown to be sensitive to the surface topography of the implant. Metallic surface modification techniques such as acid etching or grit-blasting with roughness values on the order of a few microns have been shown to increase the amount of *in vitro* VEGF and PDGF being expressed at a wound site via increased platelet adhesion [52]. Similarly, the introduction of nanoscale features on an implant surface has shown stark

increases in vascular regeneration after only seven days of *in vivo* growth [53]. Independent of any pseudohypoxic response, the topography of the alginate gels has a similar magnitude to that of a grit-blasted or acid-etched metallic surface. The cobblestone-like morphology of the films provide elements favourable for prospective aid in both osteogenesis and angiogenesis. Ultimately, however, the xerogel films are designed to interface with biological entities within hydrated environments.

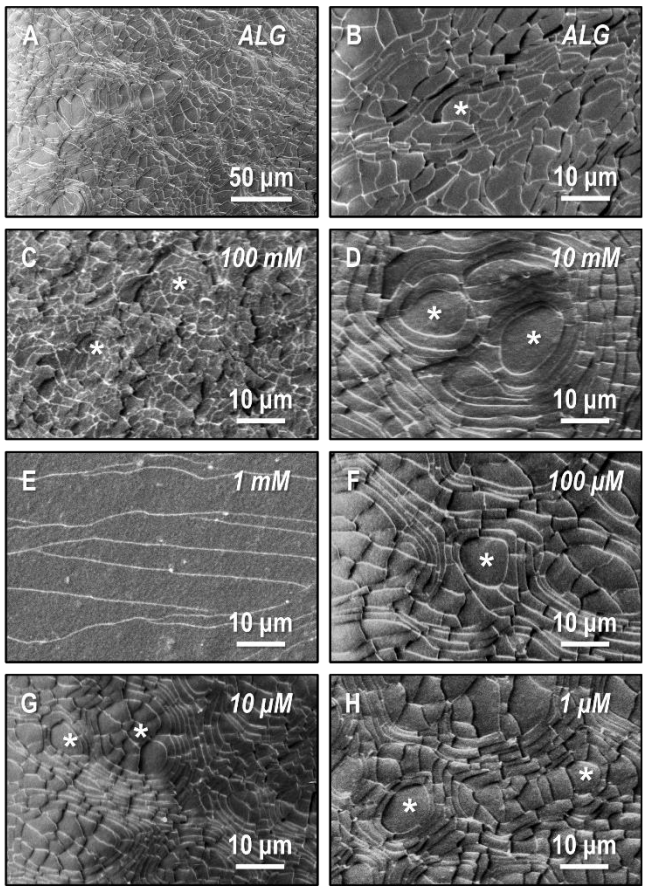

Figure 3: *SEM of dehydrated succinate xerogels on metallic substrates with the following concentrations of succinate: (A-B) Alginate (ALG) only; (C) 100 mM; (D) 10 mM; (E) 1 mM; (F) 100 µM; (G) 10 µM; (H) 1 µM. Xerogels display a complex, fragmented surface topography favourable for cellular adhesion with a common concentric pattern centred at the regions denoted with asterisks.*

SEM of hydrated materials is often challenging due to the high-vacuum environment within the microscope. Treatment with room-temperature ionic liquids has previously been shown to enable imaging of hydrated biological materials in a manner that preserves delicate microscale structures [54,55] where choline lactate pre-treatments cause minimal surface damage to hydrated polymeric structures [56,57]. While the surface topography of the succinate-alginate gels is favourable in dehydrated xerogel form, *in vitro* testing environments and *in vivo* applications of succinate-based gels are necessarily hydrated. To assess the effect of gel swelling on surface topography, the xerogels were rehydrated with a solution of room temperature choline lactate solution for additional SEM. A markedly different surface structure was seen in the hydrated gels compared to their xerogel state. A micrograph of the rehydrated alginate-only gel is seen in Figure 4A, where

surface patterning on the microscale is equally abundant to the dehydrated state but there is a loss in mesoscale roughness. Here, the micro-wrinkled architecture of the dehydrated xerogel is evident in isolated regions, where wrinkles are also evident in gels regardless of succinate content. In some regions at higher magnification (Figure 4H), the faint cobblestone pattern observed in the dehydrated xerogels can also be seen underneath this wrinkled exterior of the rehydrated gel – albeit not ubiquitously. Prolonged exposure to the microscope vacuum may play a role in partially contracting the gel to form these cobblestone and wrinkled shapes, but the coexistence of sub-surface cobblestone patterns and wrinkled surfaces indicate that the microscale surface topography of the alginate may be sensitive to environmental factors. In both the rehydrated alginate-only and rehydrated succinate-alginate gels, the multiscale features should be both angiogenic and osteogenic in nature. It is clear that the surface morphology of the alginate can differ depending on whether imaging is conducted in rehydrated or xerogel form and this highlights the necessity of hydrated imaging techniques to properly assess hydrogel, xerogel, and aerogel surface topography. The transition from fragmented to micro-wrinkled during xerogel rehydration is something that warrants further study during in vivo swelling of the gels and could posit interesting conclusions on the kinetics and adaptive response of early cell adhesion.

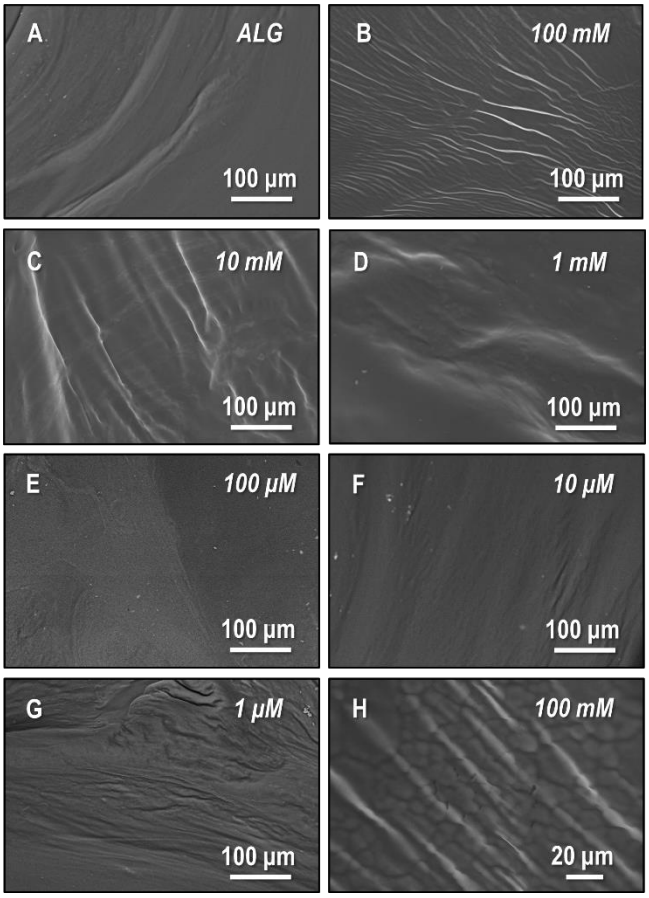

Figure 4: *SEM of hydrated succinate gels using choline lactate ionic liquid, showing films with concentrations of succinate:(A) Alginate (ALG) only; (B) 100 mM; (C) 10 mM; (D) 1 mM; (E) 100 µM; (F) 10 µM; (G) 1 µM. Imaging in the hydrated state reduces the presence of the fragmented topography and instead introduces a micro-wrinkled surface texture. The persisting features in*

the rehydrated state show promise for improving cellular activity on an alginate-coated metallic surface. (H) In some instances, underlying topography is visible underneath the outer surface.

3.2 Succinate release profiles and surface behaviour

Since the aim of the films is for driving neovascularization to an implant interface, it is important to establish release profiles of succinate during rehydration and measure the cellular response in a succinate-enriched environment. Neovascularization at the implant interface occurs very early in the osteogenic cascade, where partial vascular ingrowth into a murine defect is visible after only three days [18] and a vascular network can span the entirety of a defect after one week [58]. It is important that the pseudohypoxic gels are eluting succinate in a rapid-release format to help build this early provisional vascular network after implantation. As a conjugate base for succinic acid, disodium succinate release from the gel results in a pH increase in the absence of buffer solution. pH measurements were recorded during alginate-succinate gel release studies at succinate concentrations between 100 mM and 1 μM. Short-term succinate release profiles across the first 100 min of rehydration can be seen in Figure 5A and longer-term release profiles over 36 hr can be found in Figure S1. All gels showed an increase in average pH over alginate films as a result of succinate addition.

Trends in pH release can be found in succinate concentrations of 10 mM or below. At 10 mM, the maximum pH of disodium succinate in the deionized water was measured at 9.8. At lower succinate concentrations (1 mM, 100 μM, 10 μM, and 1 μM), the peak pH was measured at 9.0 ± 0.1, 8.1 ± 0.1, 7.8 ± 1.2, and 7.3 ± 0.9 respectively. For every tenfold reduction in succinate concentration within the xerogel, the resulting peak hydroxyl concentration in the solution diminished by less than tenfold. Where the pH shift in these experiments is appreciable, natural buffering effects in an *in vivo* setting should help maintain a physiological pH. Gels loaded with 100 mM of succinate showed lower peak pH than that of the 10 mM concentrations and a similar magnitude to the 1 mM gels (Figure S1), where a decline was also observed after the early spike in solution pH. This could suggest that high succinate content within the xerogel induces some structural change that is not visible in SEM.

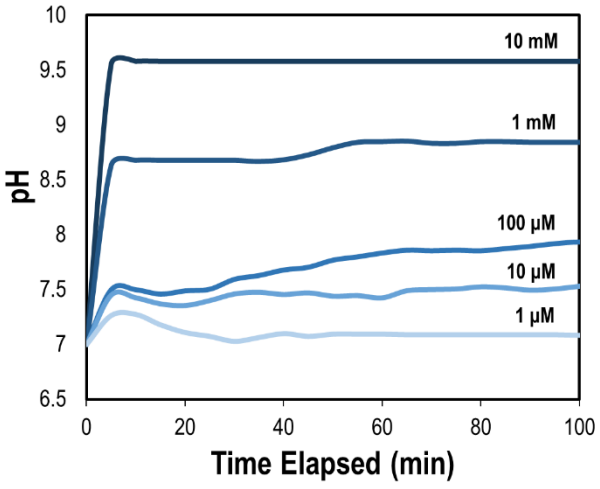

Figure 5: *Short-term release profiles for alginate gels containing succinate concentrations of 10 mM, 1 mM, 100 μM, 10 μM, and 1 μM. Independent of concentration, succinate has a rapid release*

profile due to its small molecular size and weak binding within the gel. Gels with higher succinate content elevate solution pH by a greater amount.

For the 10 mM, 1 mM, and 0.1 mM gels, peak solution pH was typically observed after roughly 10 hr of immersion in deionized water, although the bulk of the disodium succinate escapes the gel within the first several minutes as all gels reached 60% of peak solution pH after only 40 min of immersion. For gels containing 10 mM of succinate or less, 95% of peak solution pH was also achieved within the first 7 hr. The rapid release profile of the succinate-laden xerogel films could facilitate early changes in the implant's local environment to affect the fracture healing cascade and signal recruitment for progenitors of both osteogenesis and angiogenesis. Where prolific vascular growth on a metallic implant material is present after only seven days of implantation and evidence of vascular branching is evident as early as three days after implantation [53], fast-releasing materials may be favourable to promote early assembly of the provisional vascular network and angiogenesis. Platelets, as an example, are known to release inflammatory mediators (including PDGF and VEGF) and are active within seconds during the wound healing process, while neutrophils can aid in increasing vascular permeability with peak activity occurring at 24 hr [59].

The cellular response is also known to be sensitive to the mechanical properties of gels in general [60]. Where the mechanical properties of calcium cross-linked alginate gels have been defined previously [61], there is a known correlation between mannuronate-to-guluronate ratio and alginate content. The lack of cross-linking in the as-deposited alginate-succinate xerogels produces a fragile gel upon rehydration (Fig. S2), with rheological properties that cannot be easily measured. The swelling ratio of gels has been correlated to mechanical properties by Subramani et al., who note that softer gels tend to have a higher equilibrium swelling ratio [62]. Swelling ratios for the alginate-succinate gels after 60 min exposure to deionized water are shown in Fig. S2, with all gels behaving consistently.

To govern the mechanical stability of these alginate films, metal-carboxylate complexes in alginate specifically can form via ionic affinity, unidentate coordination, bidentate chelation, or bidentate bridging depending on the characteristics of the metal itself (including its pre-treatments) [63] and the mannuronate-to-guluronate ratio of the alginate – in part due to steric factors [64]. Structural modification of polymers shows the importance of hydrogen bonding in the corresponding adhesion properties to titania [65] – a material that passively forms at the exterior of titanium implants. The nature of polymer-metal adhesion, and especially hydroxyl and carboxyl groups, contributes to the mechanical properties of the interface – helping govern the mechanical stability of a hydrogel- or xerogel-based coating.

FTIR of the alginate-succinate xerogels shows similar spectra in the succinate concentration range of 1 μM to 100 mM (Figure 6A-B). The presence of hydroxyl groups (Figure 6C and 6E) and carboxyl salts (Figure 6D) [66] are both promising as prospective sites to promote metal-polymer adhesion. Within the O-H stretching band (~3300 cm^{-1}) there is a slight shift where higher concentrations of succinate show less absorbance. As the disodium sodium succinate consists of an aliphatic chain with fewer hydroxyl groups than the alginate backbone, the decrease in infrared absorbance is likely attributed to higher fractions of succinate within the xerogel. Absorbance corresponding to carboxylate salts (~1600 cm^{-1}) is less clear due to the possible retention of water during synthesis. The 100 mM succinate xerogel appears to show less absorbance in this region,

but all other gels show similar structure. Similarly, a region associated with C-H and O-H bending (1410 cm^{-1}) appears similar for all xerogels.

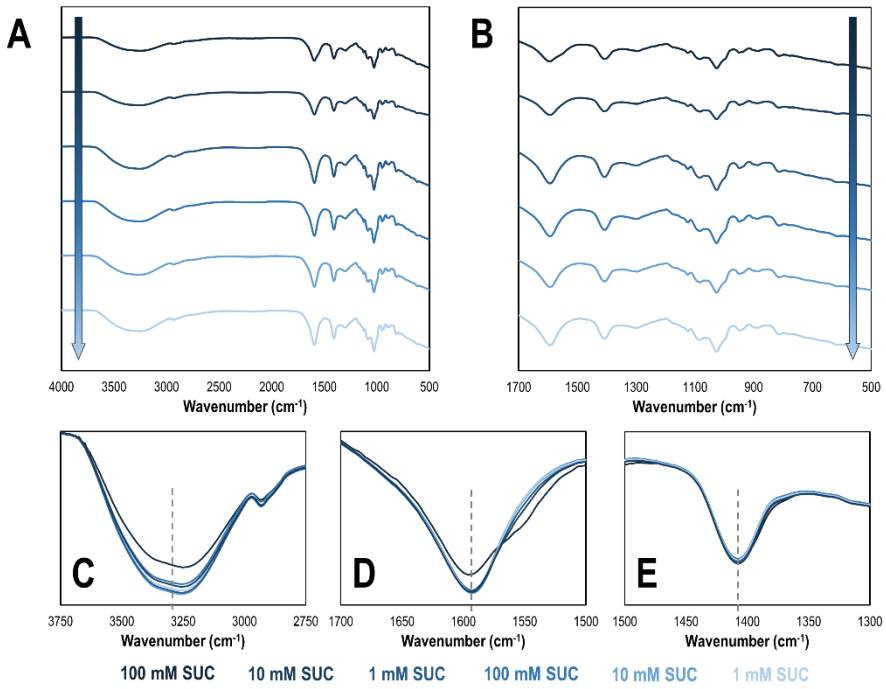

Figure 6: *Fourier-transform infrared spectroscopy of alginate-succinate xerogels. (A-B) Transmittance spectra within the range of 4000-500 cm^{-1} and inset of the fingerprint region. (C) Overlaid spectra highlighting O-H stretching. (D) Overlaid spectra near the region of residual water and carboxylate salts. (E) Overlaid spectra of C-H and O-H bending absorption.*

It may be beneficial in the future to attempt cross-linking within the alginate gel to alter the mechanical properties of the xerogels or tune succinate release profiles with other organic binders to create slow-releasing forms of temporally-relevant pseudohypoxic environments at the implant exterior. Additionally, co-functionalization using antibacterial agents or other biomolecules may result in favourable *in vivo* behaviour.

3.3 In vitro Saos-2 culture

The development of early capillaries within the bone defect is directly related to osteogenic differentiation near the implant, where clustering of RUNX2-positive mesenchymal cells or pericytes can occur around the capillary wall [67]. As succinate is released into the peri-implant space, these is potential for interaction with both pre-existing bone tissue and newly differentiating osteoblastic progenitors. For the latter, it is important to understand how a near-bolus release of succinate can interact with osteoblasts near an implant surface. We used the Saos-2 cell line here to quantify the *in vitro* metabolic activity of cells with osteoblastic behaviour as they interact with the succinate-loaded xerogels after one and four days of culture.

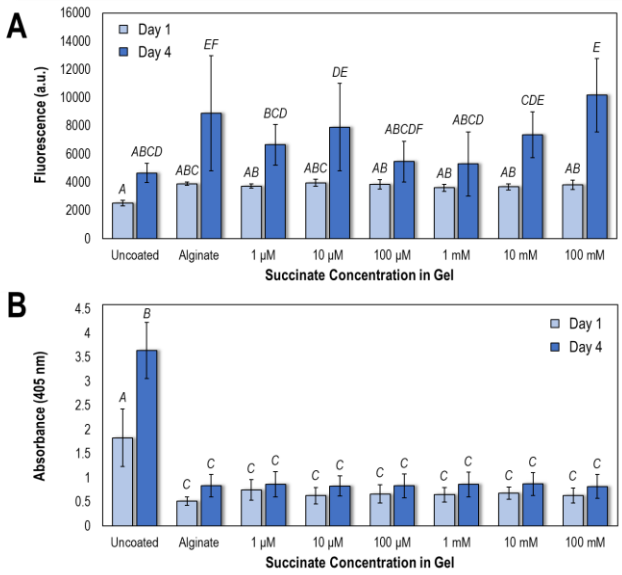

Figure 7: *Cytocompatibility of alginate-succinate gels using Saos-2 osteosarcoma cells. (A) Metabolic activity of Saos-2 cells. Alginate-succinate gels are able to sustain in vitro growth of osteoblast-mimicking cells and statistically outperform uncoated polystyrene control substrates after one day. (B) Despite increased metabolic rates, the addition of alginate appears to reduce the production of alkaline phosphatase. Significance defined as $p < 0.05$. Groups sharing a letter are not statistically different from one another.*

Measurements of metabolic activity for osteoblast-mimicking cells grown on alginate-succinate xerogel films and polystyrene control surfaces are shown in Figure 7A. All coatings showed statistically significant increases in metabolic activity compared to the uncoated polystyrene after only one day of culture, which is consistent with the fast-acting release mechanism of the gels. The 100 mM succinate, 10 mM succinate, 10 µM succinate, and succinate-deficient rehydrated gels all showed increases in cellular metabolism from day one to day four of *in vitro* culture, suggesting that succinate inclusion within the gels does not compromise the cytocompatibility of the material with respect to newly derived osteoblasts or pre-existing bone tissue, and can instead promote cellular proliferation of osteoblasts. This is important as it suggests minimal damage to surrounding tissue should succinate induce a pseudohypoxic environment and further promotes osteogenesis on an implant surface. Despite the common influence of pH on fluorescence intensity [68] and the recommended assay pH of 7.4, the optical characteristics of resazurin-based assays have been observed to change more drastically in acidic conditions rather than basic conditions [69]. The addition of sodium bicarbonate (2.2 g/L) as a buffering agent in the culture media should help prevent against pH-dependent fluorescence shifts, especially in the cultures conducted on gels with a succinate concentration in the micromolar range, but could lead to inflated fluorescence signal in high-millimolar concentrations of succinate. The osteoblast lineage appears to be highly resilient in the presence of exogenous succinate at or below 100 mM and should readily support osteoblastic proliferation within pseudohypoxic environments.

Alkaline phosphatase production was reduced in all cells cultured on alginate and alginate-succinate xerogel surfaces compared to tissue-culture polystyrene (Figure 7B). Rehydration of the

alginate xerogels produces a substrate with lower stiffness than the native polystyrene surfaces. As ALP production is often controlled by matrix stiffness [70], the reduction in alkaline phosphatase production can therefore be attributed to the presence of the alginate xerogels in each well. The addition of disodium succinate does not appear to alter ALP production compared to the base alginate xerogel. One of the main roles of ALP is to regulate phosphates and deactivate pyrophosphate as a mineralization inhibitor [71]. Considering that neovascularization is an early-stage biological process, and the formation of mineralized matrix is, comparatively, a later-stage phenomenon [72], the early downregulation of ALP may be tolerable until the rapid release of succinate is complete. By tuning the properties of alginate or other matrix materials to degrade after the initial fast release of succinate, a bare metallic implant substrate can be left behind to restore the typical levels of ALP production associated with stiff materials.

3.4 In vitro endothelial culture

In light of their potentially suitable surface structure and osteocompatibility, it is necessary to quantify the vascular development and endogenous protein production occurring as a result of endothelial exposure to the succinate. Human umbilical vein endothelial cells (HUVECs) were cultured in the presence of succinate-conditioned media to assess the effects of locally elevated succinate on neovascularization potential. Since the rapid release profile of the alginate-succinate gels enables elevated succinate levels within the first 7 hr, early characterization of endothelial cell behaviour offers insight as to how vascular development can occur at the implant interface.

Total protein content after 48 hours was assessed using a bicinchoninic acid (BCA) protein assay, as shown in Figure 8. Disodium succinate concentrations of 0, 1, 10, and 100 μM in endothelial growth culture medium were used to evaluate the potency of succinate in eliciting hypoxia-mediated HUVEC activity. Supplementing the media with disodium succinate and culturing on Matrigel-coated plates instead of culturing HUVECs onto the xerogels directly allows for the succinate to take effect while mitigating any confounding effects relating to substrate stiffness and topography during tube formation. Culture environments containing 1 μM or 10 μM of succinate exhibited significantly increased levels of total protein expression. An insignificant difference in protein levels between treatment and control environments is observed when the concentration is increased to 100 μM of succinate. Stabilized HIF-1α from pseudohypoxia can result in different cell fates depending on hypoxic severity and protein concentrations, ranging from enhanced cell survival to the initiation of apoptosis [73]. Hypoxia-induced cellular fates could change following succinate exposure, with differences in protein expression arising from the added succinate. Where the 10 μM succinate concentration resulted in an increase of Saos-2 cell proliferation, it is also possible that the increase in total protein content at this concentration in the HUVEC culture can be attributed in part to proliferative effects.

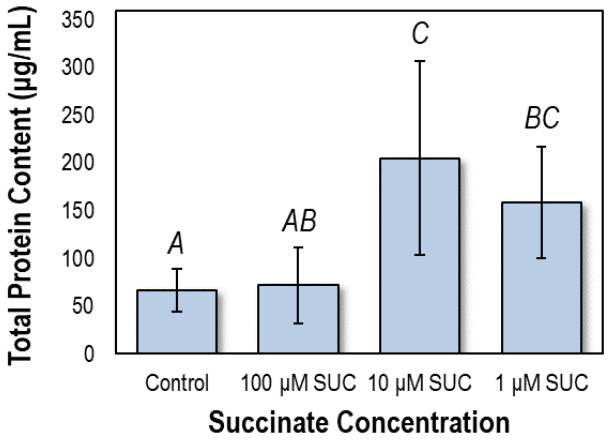

Figure 8: *Total protein content from BCA assay of HUVECs treated with succinate-added media after 48 hr. Succinate concentrations of 10 µM and 1 µM in the culture media promote early endogenous protein production in the cells. Significance defined as $p < 0.05$. Groups sharing a letter are not statistically different from one another.*

Tube thickness maps overlaid onto bright-field optical micrographs of HUVEC cells (Figure 9A) further demonstrate trends observed in Figure 8. The tube-forming behaviour of HUVEC cells is evidently modified by the presence of succinic acid salt in solution. Although cells treated with 1 and 10 µM show decreased vascular branching compared to succinate-free controls (Figure S3) along with lower vascularized areas (Figure 9B), there is circumstantial evidence to support earlier tube formation in both cases. The reduced vascularized area in the 1 µM and 10 µM succinate concentrations after 48 hr is inversely correlated to the total protein content measured at this time point, suggesting that factors other than cell count are driving the difference in lysate protein content and that succinate-enhanced media in the low-micromolar range is able to alter molecular pathways. At 100 µM, the branching behaviour at 6 hr is comparable to succinate-free HUVECs but also declines at later time points. At 1 and 10 µM, it is possible that the reduced branching behaviour can be explained by an early onset of cell anastomosis and stabilization of the endothelial-to-endothelial junctions at 6 hr, 24 hr, and 48 hr timepoints investigated here. The quiescent layer of endothelial cells is known to maintain a more dormant phenotype unless acted on by pro-angiogenic macromolecules, which activates only select cells in the local microenvironment and encourage outward branching from parental vessels [74]. Where total protein content is highest at 1 and 10 µM, it is assumed that any corresponding degree of HIF-1α stabilization should lead to earlier shifts in phenotypic behaviour, cell anastomosis, and a more mature form of vascularization at these time points in an *in vitro* setting. Where relevant concentrations of cobalt chloride as a known pseudohypoxic agent are often within the micromolar range to induce angiogenic behaviour [75], we show that similar concentrations of succinate can induce protein production.

Moreover, improving vascular permeability in the healing cascade holds promise for increasing macromolecular transport of growth factors, stem cells, and oxygen-rich blood to the implant site. Upregulation of pro-angiogenic factors in the VEGF family have been associated with both increased vascular permeability and vascular diameter [76]. In the work presented here, the HUVEC

tube network is observed as a spindly vascular plexus at the 6 hr time point and expands as the process of tubulogenesis continues (Table 1 and Figure S4). Sustained growth in vessel diameter is only observed at the 48 hr time point in the test groups of 1 and 10 µM succinate, where the control and 100 µM test groups both fail to coarsen at the later endpoint. The succinate-free media increased the vessel diameter after only 24 hr but regressed to a non-significant value at the 48 hr mark. As cord-hollowing mechanisms during lumen formation in tubulogenesis can result in thickening of the primitive single-celled vascular network to two or more cells in diameter [77], it is possible that the sustained expansion at 48 hr is evidence of post-angiogenic perfusability in the pseudohypoxic environment.

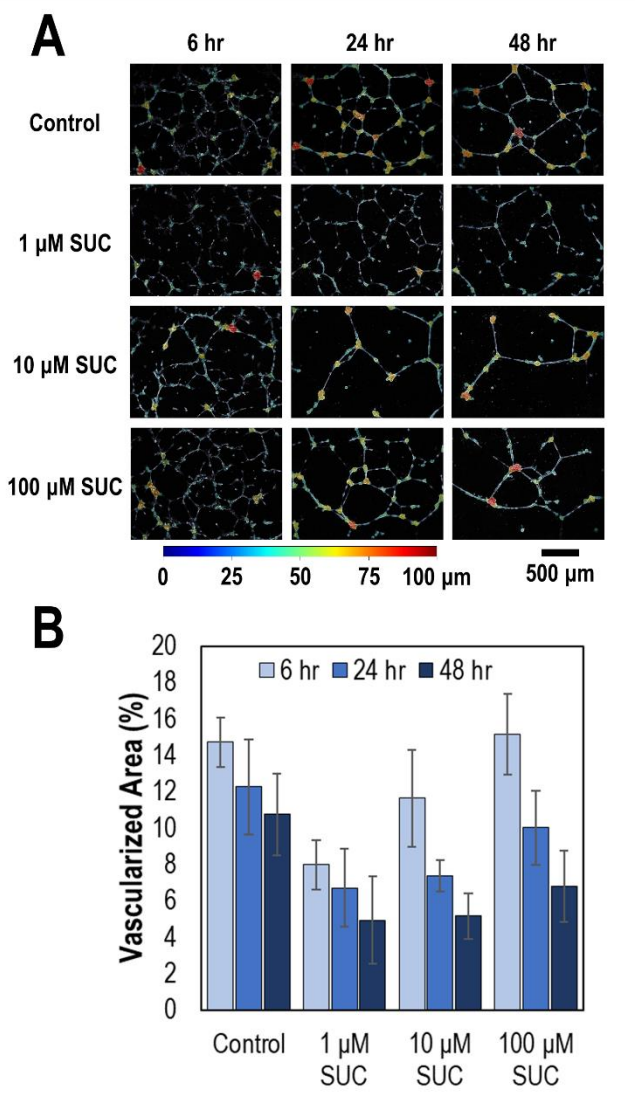

Figure 9: *(A) Thickness maps of HUVEC tube formation following 6, 24, and 48 hr of culture in succinate-supplemented culture media. Tubes are narrow and tortuous at early timepoints but coarsen over time as a result of lumen formation and anastomosis. Evolution from the provisional network at 6 hr into a coarser network at 24 hr is more evident in the 100 µM and 10 µM succinate concentrations, while many nodes appear similar in the control and 1 µM groups. (B) A net*

decrease in vascularized area is seen in all cases, with lower initial vascularized areas at succinate concentrations of 1 μM and 10 μM.

Table 1: *Average HUVEC tube width and evolution across 6, 24, 48 hr study periods. Pseudohypoxic treatments corresponding to higher total protein content (1 and 10 μM) are consistent with sustained tube widening between 6 hr and 48 hr (n = 4).* * *Statistical significance defined as p < 0.05.*

Culture Condition	Time (hr)	Tube Width (μm)	Change from 6 hr
Control	6	29.2 ± 1.9	–
	24	37.5 ± 2.1	+ 28.4%*
	48	32.5 ± 2.1	+ 11.3%
1 μM SUC	6	23.1 ± 1.4	–
	24	27.5 ± 1.4	+ 19.0%
	48	29.5 ± 1.7	+ 27.7%*
10 μM SUC	6	26.7 ± 1.5	–
	24	34.3 ± 1.9	+ 28.4%
	48	38.0 ± 2.4	+ 42.3%*
100 μM SUC	6	31.2 ± 1.8	–
	24	38.4 ± 2.1	+ 23.1%
	48	34.7 ± 2.5	+11.2%

Despite the longer-term benefit of adding the 1 and 10 μM of succinate to the culture media, it is possible that undesirable vessel morphogenesis occurs at higher concentration. Cells treated with 100 μM succinic acid form early networks with large tube diameters (Table 1) but tubes do not grow at later time points. It is possible that, in these highly pseudohypoxic environments, vessels are becoming hyperpermeable or 'leaky' in nature [78] in part by disassembling endothelial adherens junctions [79]. It is also possible that the induction of apoptotic signalling takes place in environments where more severe hypoxia is present [73]. In either case, exposure to 100 μM of succinate appears less beneficial than 1 or 10 μM, leading to reduced intracellular protein content and less permeable vessels in the first 48 hours.

The lack of longer-term vascular stability in the 100 μM and control groups may also be attributed to the complexity of vascular morphogenesis and limitations of *in vitro* modelling. Specifically, the importance of mural cells and pericyte recruitment in the tubulogenesis cannot be observed in endothelial-only systems. Endothelial-pericyte co-cultures have previously shown that the recruitment of pericytes to the site of endothelial tube formation results in enhanced secretion and deposition of basement membrane matrix, which is integral to vessel maturation. Further, the absence of pericytes following early tube formation reportedly leads to tube instability and regression [80]. An added benefit of introducing pericytes is a potential osteogenic progenitor source, where an abundance of PDGF-BB is one mechanism for improved osseointegration [81] via potential pericyte recruitment, maturation, and detachment [82]. Examining the levels of PDGF-BB in both

the culture media and cell lysate solution during HUVEC culture (Figure 10A) shows high levels of PDGF-BB within the extracellular domain in both control media and succinate-conditioned media. In its role as an osteoblast mitogen and chemoattractant, PDGF-BB can aid in the recruitment of early osteoblasts at a defect site. However, cytokines such as PDGF have known complications with respect to osteopontin (OPN) production [83], where OPN can be more abundant in certain osteoblastic phenotypes and the resulting OPN influences extracellular matrix mineralization patterns in the bone tissue [84]. Levels of VEGF-A content in the intracellular and extracellular domains appear to be consistent with HUVEC cells cultured in the control media (Figure 10B). After 48 hr, it is possible that some intracellular VEGF has been degraded as a part of the early response necessary for cell survival. Since the culture media formulation contains both VEGF and PDGF, it is possible that HUVECs exposed to the succinate *in vitro* are sustained by the media as an exogenous source rather than endogenously producing the proliferative growth factors. Follow-up studies using Medium-199 or other media formulations without growth factor addition could help decouple the endogenous and exogenous sources. Potential exogenous sources *in vivo* include mesenchymal stem cells [85], platelets [86], and neutrophils [87] which all secrete angiogenic factors and are present early in the fracture healing cascade.

Despite the lack of *in vitro* VEGF and PDGF upregulation here, the phenomenon of HIF-1α stabilization is well-documented elsewhere [88–91]. However, upregulation of angiogenic factors by succinate is possible in mechanisms other than the HIF-1α pathway. Instead of using the SLC13 family of transporters to facilitate succinate transport across cell membranes in a sodium-dependent manner [92], work from Sapieha et al. has shown that succinate-driven activation of the G-protein coupled receptor GPR91 can also initiate the angiogenic cascade in the retina [93]. Where both of these mechanisms rely on a supply of extracellular succinate, delivery strategies like the alginate-succinate coating presented here afford a prospective means for early angiogenesis at the bone-implant interface.

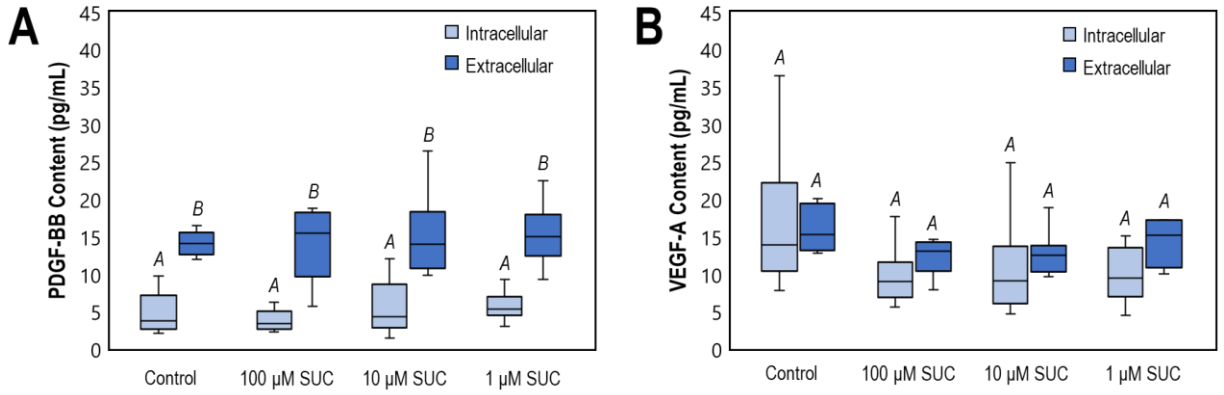

Figure 10: *Growth factor content in the succinate conditioned media (extracellular) and the cell lysate solution (intracellular) components following HUVEC culture for (A) PDGF-BB and (B) VEGF-A. Groups sharing a letter are not statistically different from one another.*

An important confounding factor to these results is the aspect of time. Figure S4 shows that different treatment groups showed differing vessel diameter distributions over the first 48 hours following succinate addition, however, tube formation can begin to occur *in vitro* as early as 2-6

hr with peak tube formation reported in the range of 3-12 hr depending on the presence of angiogenic stimuli [94]. The rapid changes in the cellular environment shown in Figure 9 suggests that neovascularization demands timely availability of vessel-forming resources to develop from a thin, lumen-free network into a more mature network. Further to this claim is the possibility that succinate-induced hypoxia influences the time at which these resources are needed to form viable vasculature before regression ensues.

4 Conclusions

Alginate-based xerogels produced a surface film capable of rapid release of disodium succinate which may create a local pseudohypoxic environment for faster neovascularization in the vicinity of implants. By adding succinate to the gel on the order of 1 or 10 μM, an increase in the amount of stabilized protein and branching behaviour in HUVEC cells occurred. Succinate concentrations in the low-μM range encouraged the expansion of the provisional vascular network formed *in vitro* by HUVECs without risk of hyperpermeability or cytotoxic effects. Moreover, the rapid dosing of succinate below 100 mM did not inhibit the proliferation of osteoblast-like Saos-2 cells. Therefore, based on the response of HUVEC and Saos-2 cells, the succinate release showed promise for providing short-term angiogenic benefits during early timepoints for vessel formation at an implant surface. Future work could assess the co-functionalization of other macromolecules to improve early implant stability, while *in vitro* experiments should explore co-culture environments to better replicate vessel formation, and ultimately investigation of *in vivo* vessel development and downstream implications on early osteogenesis is needed.

5 Acknowledgements

Work was performed at the Canadian Centre for Electron Microscopy, the Biointerfaces Institute, and the Centre for Microbial Chemical Biology at McMaster University. Select figures were made using BioRender. The authors would like to acknowledge funding from the Natural Sciences and Engineering Research Council of Canada (RGPIN-2020-05722) and Canada Research Chairs Program and the Foshan Science and Technology Innovation Project (No. 2018IT100212).

References

(1) Albrektsson, T.; Johansson, C. Osteoinduction, Osteoconduction and Osseointegration. *Eur Spine J* 2001, *10* (Suppl 2), S96–S101. https://doi.org/10.1007/s005860100282.

(2) Albrektsson, T.; Brånemark, P.-I.; Hansson, H.-A.; Lindström, J. Osseointegrated Titanium Implants: Requirements for Ensuring a Long-Lasting, Direct Bone-to-Implant Anchorage in Man. *Acta Orthop Scand* 1981, *52* (2), 155–170.

(3) D'Elia, A.; Deering, J.; Clifford, A.; Lee, B. E. J.; Grandfield, K.; Zhitomirsky, I. Electrophoretic Deposition of Polymethylmethacrylate and Composites for Biomedical Applications. *Colloids Surfaces B Biointerfaces* 2019, *188*, 110763. https://doi.org/10.1016/j.colsurfb.2019.110763.

(4) Clifford, A.; D'Elia, A.; Deering, J.; Lee, B. E. J.; Grandfield, K.; Zhitomirsky, I. Electrochemical Fabrication and Characterization of Pectin Hydrogel Composite Materials for

Bone Tissue Repair. *Acs Appl Polym Mater* 2020, *2* (8), 3390–3396. https://doi.org/10.1021/acsapm.0c00480.

(5) Deering, J.; Clifford, A.; D'Elia, A.; Zhitomirsky, I.; Grandfield, K. Composite Dip Coating Improves Biocompatibility of Porous Metallic Scaffolds. *Mater Lett* 2020, *274*, 128057. https://doi.org/10.1016/j.matlet.2020.128057.

(6) Catauro, M.; Bollino, F.; Giovanardi, R.; Veronesi, P. Modification of Ti6Al4V Implant Surfaces by Biocompatible TiO2/PCL Hybrid Layers Prepared via Sol-Gel Dip Coating: Structural Characterization, Mechanical and Corrosion Behavior. *Mater Sci Eng C* 2017, *74*, 501–507. https://doi.org/10.1016/j.msec.2016.12.046.

(7) Cao, L.; Ullah, I.; Li, N.; Niu, S.; Sun, R.; Xia, D.; Yang, R.; Zhang, X. Plasma Spray of Biofunctional (Mg, Sr)-Substituted Hydroxyapatite Coatings for Titanium Alloy Implants. *J Mater Sci Technol* 2019, *35* (5), 719–726. https://doi.org/10.1016/j.jmst.2018.10.020.

(8) Vercaigne, S.; Wolke, J. G. C.; Naert, I.; Jansen, J. A. Histomorphometrical and Mechanical Evaluation of Titanium Plasma-spray-coated Implants Placed in the Cortical Bone of Goats. *J Biomed Mater Res* 1998, *41* (1), 41–48. https://doi.org/10.1002/(sici)1097-4636(199807)41:1<41::aid-jbm5>3.0.co;2-q.

(9) Giavaresi, G.; Ambrosio, L.; Battiston, G. A.; Casellato, U.; Gerbasi, R.; Finia, M.; Aldini, N. N.; Martini, L.; Rimondini, L.; Giardino, R. Histomorphometric, Ultrastructural and Microhardness Evaluation of the Osseointegration of a Nanostructured Titanium Oxide Coating by Metal-Organic Chemical Vapour Deposition: An in Vivo Study. *Biomaterials* 2004, *25* (25), 5583–5591. https://doi.org/10.1016/j.biomaterials.2004.01.017.

(10) Cabañas, M. V.; Vallet-Regí, M. Calcium Phosphate Coatings Deposited by Aerosol Chemical Vapour Deposition. *J Mater Chem* 2003, *13* (5), 1104–1107. https://doi.org/10.1039/b301435e.

(11) Bumgardner, J. D.; Wiser, R.; Gerard, P. D.; Bergin, P.; Chestnutt, B.; Marini, M.; Ramsey, V.; Elder, S. H.; Gilbert, J. A. Chitosan: Potential Use as a Bioactive Coating for Orthopaedic and Craniofacial/Dental Implants. *J Biomaterials Sci Polym Ed* 2003, *14* (5), 423–438. https://doi.org/10.1163/156856203766652048.

(12) Leedy, M. R.; Martin, H. J.; Norowski, P. A.; Jennings, J. A.; Haggard, W. O.; Bumgardner, J. D. Use of Chitosan as a Bioactive Implant Coating for Bone-Implant Applications. *Adv Polym Sci* 2011, 129–165. https://doi.org/10.1007/12_2011_115.

(13) Yin, X.; Yang, C.; Wang, Z.; Zhang, Y.; Li, Y.; Weng, J.; Feng, B. Alginate/Chitosan Modified Immunomodulatory Titanium Implants for Promoting Osteogenesis in Vitro and in Vivo. *Mater Sci Eng C* 2021, *124*, 112087. https://doi.org/10.1016/j.msec.2021.112087.

(14) Lv, H.; Chen, Z.; Yang, X.; Cen, L.; Zhang, X.; Gao, P. Layer-by-Layer Self-Assembly of Minocycline-Loaded Chitosan/Alginate Multilayer on Titanium Substrates to Inhibit Biofilm Formation. *J Dent* 2014, *42* (11), 1464–1472. https://doi.org/10.1016/j.jdent.2014.06.003.

(15) Chua, P.-H.; Neoh, K.-G.; Kang, E.-T.; Wang, W. Surface Functionalization of Titanium with Hyaluronic Acid/Chitosan Polyelectrolyte Multilayers and RGD for Promoting Osteoblast Functions and Inhibiting Bacterial Adhesion. *Biomaterials* 2008, *29* (10), 1412–1421. https://doi.org/10.1016/j.biomaterials.2007.12.019.

(16) Valverde, A.; Pérez-Álvarez, L.; Ruiz-Rubio, L.; Olivenza, M. A. P.; Blanco, M. B. G.; Díaz-Fuentes, M.; Vilas-Vilela, J. L. Antibacterial Hyaluronic Acid/Chitosan Multilayers onto Smooth and Micropatterned Titanium Surfaces. *Carbohyd Polym* 2019, *207*, 824–833. https://doi.org/10.1016/j.carbpol.2018.12.039.

(17) Tibbitt, M. W.; Anseth, K. S. Hydrogels as Extracellular Matrix Mimics for 3D Cell Culture. *Biotechnol Bioeng* 2009, *103* (4), 655–663. https://doi.org/10.1002/bit.22361.

(18) Khosravi, N.; Maeda, A.; DaCosta, R. S.; Davies, J. E. Nanosurfaces Modulate the Mechanism of Peri-Implant Endosseous Healing by Regulating Neovascular Morphogenesis. *Commun Biology* 2018, *1* (1). https://doi.org/10.1038/s42003-018-0074-y.

(19) Kanczler, J.; Oreffo, R. Osteogenesis and Angiogenesis: The Potential for Engineering Bone. *European Cells Mater* 2008, *15*, 100–114. https://doi.org/10.22203/ecm.v015a08.

(20) Street, J.; Bao, M.; deGuzman, L.; Bunting, S.; Peale, F. V.; Ferrara, N.; Steinmetz, H.; Hoeffel, J.; Cleland, J. L.; Daugherty, A.; Bruggen, N. van; Redmond, H. P.; Carano, R. A. D.; Filvaroff, E. H. Vascular Endothelial Growth Factor Stimulates Bone Repair by Promoting Angiogenesis and Bone Turnover. *Proc National Acad Sci* 2002, *99* (15), 9656–9661. https://doi.org/10.1073/pnas.152324099.

(21) Mayr-Wohlfart, U.; Waltenberger, J.; Hausser, H.; Kessler, S.; Günther, K.-P.; Dehio, C.; Puhl, W.; Brenner, R. E. Vascular Endothelial Growth Factor Stimulates Chemotactic Migration of Primary Human Osteoblasts. *Bone* 2002, *30* (3), 472–477. https://doi.org/10.1016/s8756-3282(01)00690-1.

(22) Parajó, Y.; d'Angelo, I.; Welle, A.; Garcia-Fuentes, M.; Alonso, M. J. Hyaluronic Acid/Chitosan Nanoparticles as Delivery Vehicles for VEGF and PDGF-BB. *Drug Deliv* 2010, *17* (8), 596–604. https://doi.org/10.3109/10717544.2010.509357.

(23) Chung, H.-J.; Kim, J.-T.; Kim, H.-J.; Kyung, H.-W.; Katila, P.; Lee, J.-H.; Yang, T.-H.; Yang, Y.-I.; Lee, S.-J. Epicardial Delivery of VEGF and Cardiac Stem Cells Guided by 3-Dimensional PLLA Mat Enhancing Cardiac Regeneration and Angiogenesis in Acute Myocardial Infarction. *J Control Release* 2015, *205*, 218–230. https://doi.org/10.1016/j.jconrel.2015.02.013.

(24) Ferrara, N. VEGF and the Quest for Tumour Angiogenesis Factors. *Nat Rev Cancer* 2002, *2* (10), 795–803. https://doi.org/10.1038/nrc909.

(25) Ehrbar, M.; Djonov, V. G.; Schnell, C.; Tschanz, S. A.; Martiny-Baron, G.; Schenk, U.; Wood, J.; Burri, P. H.; Hubbell, J. A.; Zisch, A. H. Cell-Demanded Liberation of VEGF121 From Fibrin Implants Induces Local and Controlled Blood Vessel Growth. *Circ Res* 2004, *94* (8), 1124–1132. https://doi.org/10.1161/01.res.0000126411.29641.08.

(26) Zisch, A. H.; Schenk, U.; Schense, J. C.; Sakiyama-Elbert, S. E.; Hubbell, J. A. Covalently Conjugated VEGF–Fibrin Matrices for Endothelialization. *J Control Release* 2001, *72* (1–3), 101–113. https://doi.org/10.1016/s0168-3659(01)00266-8.

(27) Silva, E. A.; Mooney, D. J. Effects of VEGF Temporal and Spatial Presentation on Angiogenesis. *Biomaterials* 2010, *31* (6), 1235–1241. https://doi.org/10.1016/j.biomaterials.2009.10.052.

(28) Pidgeon, G. P.; Barr, M. P.; Harmey, J. H.; Foley, D. A.; Bouchier-Hayes, D. J. Vascular Endothelial Growth Factor (VEGF) Upregulates BCL-2 and Inhibits Apoptosis in Human and Murine Mammary Adenocarcinoma Cells. *Brit J Cancer* 2001, *85* (2), 273–278. https://doi.org/10.1054/bjoc.2001.1876.

(29) Sano, H.; Hosokawa, K.; Kidoya, H.; Takakura, N. Negative Regulation of VEGF-Induced Vascular Leakage by Blockade of Angiotensin II Type 1 Receptor. *Arteriosclerosis Thrombosis Vasc Biology* 2006, *26* (12), 2673–2680. https://doi.org/10.1161/01.atv.0000245821.77155.c3.

(30) Lee, K. Y.; Peters, M. C.; Mooney, D. J. Comparison of Vascular Endothelial Growth Factor and Basic Fibroblast Growth Factor on Angiogenesis in SCID Mice. *J Control Release* 2003, *87* (1–3), 49–56. https://doi.org/10.1016/s0168-3659(02)00349-8.

(31) Poh, C. K.; Shi, Z.; Lim, T. Y.; Neoh, K. G.; Wang, W. The Effect of VEGF Functionalization of Titanium on Endothelial Cells in Vitro. *Biomaterials* 2010, *31* (7), 1578–1585. https://doi.org/10.1016/j.biomaterials.2009.11.042.

(32) Cleland, J. L.; Duenas, E. T.; Park, A.; Daugherty, A.; Kahn, J.; Kowalski, J.; Cuthbertson, A. Development of Poly-(d,l-Lactide–Coglycolide) Microsphere Formulations Containing Recombinant Human Vascular Endothelial Growth Factor to Promote Local Angiogenesis. *J Control Release* 2001, *72* (1–3), 13–24. https://doi.org/10.1016/s0168-3659(01)00258-9.

(33) Wu, J.; Zeng, F.; Huang, X.-P.; Chung, J. C.-Y.; Konecny, F.; Weisel, R. D.; Li, R.-K. Infarct Stabilization and Cardiac Repair with a VEGF-Conjugated, Injectable Hydrogel. *Biomaterials* 2011, *32* (2), 579–586. https://doi.org/10.1016/j.biomaterials.2010.08.098.

(34) Zhang, X.; Zhang, G.; Zhang, H.; Liu, X.; Shi, J.; Shi, H.; Yao, X.; Chu, P. K.; Zhang, X. A Bifunctional Hydrogel Incorporated with CuS@MoS2 Microspheres for Disinfection and Improved Wound Healing. *Chem Eng J* 2020, *382*, 122849. https://doi.org/10.1016/j.cej.2019.122849.

(35) Schellekens, H. Immunogenicity of Therapeutic Proteins: Clinical Implications and Future Prospects. *Clin Ther* 2002, *24* (11), 1720–1740. https://doi.org/10.1016/s0149-2918(02)80075-3.

(36) Fairbrother, W. J.; Champe, M. A.; Christinger, H. W.; Keyt, B. A.; Starovasnik, M. A. Solution Structure of the Heparin-Binding Domain of Vascular Endothelial Growth Factor. *Structure* 1998, *6* (5), 637–648. https://doi.org/10.1016/s0969-2126(98)00065-3.

(37) Wang, W.; Huang, X.; Lin, W.; Qiu, Y.; He, Y.; Yu, J.; Xi, Y.; Ye, X. Hypoxic Preconditioned Bone Mesenchymal Stem Cells Ameliorate Spinal Cord Injury in Rats via Improved Survival and Migration. *Int J Mol Med* 2018, *42* (5), 2538–2550. https://doi.org/10.3892/ijmm.2018.3810.

(38) Shweiki, D.; Itin, A.; Soffer, D.; Keshet, E. Vascular Endothelial Growth Factor Induced by Hypoxia May Mediate Hypoxia-Initiated Angiogenesis. *Nature* 1992, *359* (6398), 843–845. https://doi.org/10.1038/359843a0.

(39) Berra, E.; Benizri, E.; Ginouvès, A.; Volmat, V.; Roux, D.; Pouysségur, J. HIF Prolyl-hydroxylase 2 Is the Key Oxygen Sensor Setting Low Steady-state Levels of HIF-1α in Normoxia. *Embo J* 2003, *22* (16), 4082–4090. https://doi.org/10.1093/emboj/cdg392.

(40) Tanimoto, K.; Makino, Y.; Pereira, T.; Poellinger, L. Mechanism of Regulation of the Hypoxia-inducible Factor-1α by the von Hippel-Lindau Tumor Suppressor Protein. *Embo J* 2000, *19* (16), 4298–4309. https://doi.org/10.1093/emboj/19.16.4298.

(41) Tsuzuki, Y.; Fukumura, D.; Oosthuyse, B.; Koike, C.; Carmeliet, P.; Jain, R. K. Vascular Endothelial Growth Factor (VEGF) Modulation by Targeting Hypoxia-Inducible Factor-1alpha--> Hypoxia Response Element--> VEGF Cascade Differentially Regulates Vascular Response and Growth Rate in Tumors. *Cancer Res* 2000, *60* (22), 6248–6252.

(42) Lafforgue, P. Pathophysiology and Natural History of Avascular Necrosis of Bone. *Joint Bone Spine* 2006, *73* (5), 500–507. https://doi.org/10.1016/j.jbspin.2006.01.025.

(43) Tanaka, T.; Kojima, I.; Ohse, T.; Ingelfinger, J. R.; Adler, S.; Fujita, T.; Nangaku, M. Cobalt Promotes Angiogenesis via Hypoxia-Inducible Factor and Protects Tubulointerstitium in the Remnant Kidney Model. *Lab Invest* 2005, *85* (10), 1292–1307. https://doi.org/10.1038/labinvest.3700328.

(44) Yuan, Y.; Hilliard, G.; Ferguson, T.; Millhorn, D. E. Cobalt Inhibits the Interaction between Hypoxia-Inducible Factor-α and von Hippel-Lindau Protein by Direct Binding to Hypoxia-Inducible Factor-A*. *J Biol Chem* 2003, *278* (18), 15911–15916. https://doi.org/10.1074/jbc.m300463200.

(45) Fan, W.; Crawford, R.; Xiao, Y. Enhancing in Vivo Vascularized Bone Formation by Cobalt Chloride-Treated Bone Marrow Stromal Cells in a Tissue Engineered Periosteum Model. *Biomaterials* 2010, *31* (13), 3580–3589. https://doi.org/10.1016/j.biomaterials.2010.01.083.

(46) Lison, D.; Boeck, M. D.; Verougstraete, V.; Kirsch-Volders, M. Update on the Genotoxicity and Carcinogenicity of Cobalt Compounds. *Occup Environ Med* 2001, *58* (10), 619. https://doi.org/10.1136/oem.58.10.619.

(47) King, A.; Selak, M. A.; Gottlieb, E. Succinate Dehydrogenase and Fumarate Hydratase: Linking Mitochondrial Dysfunction and Cancer. *Oncogene* 2006, *25* (34), 4675–4682. https://doi.org/10.1038/sj.onc.1209594.

(48) Deering, J.; Presas, A.; Lee, B. E. J.; Valentin, D.; Yu, B.; Heiss, C.; Grandfield, K.; Bosbach, W. A. Response of Saos-2 Osteoblast-like Cells to Kilohertz-Resonance Excitation in Porous Metallic Scaffolds. *J Mech Behav Biomed* 2020, *106*, 103726. https://doi.org/10.1016/j.jmbbm.2020.103726.

(49) Davies, J. E. Understanding Peri-Implant Endosseous Healing. *J Dent Educ* 2003, *67* (8), 932–949. https://doi.org/10.1002/j.0022-0337.2003.67.8.tb03681.x.

(50) Pupa, P.; Apiwatsiri, P.; Sirichokchatchawan, W.; Pirarat, N.; Muangsin, N.; Shah, A. A.; Prapasarakul, N. The Efficacy of Three Double-Microencapsulation Methods for Preservation of Probiotic Bacteria. *Sci Rep-uk* 2021, *11* (1), 13753. https://doi.org/10.1038/s41598-021-93263-z.

(51) Bera, S.; Haldar, D. A Rechargeable Self-Healing Safety Fuel Gel. *J Mater Chem A* 2015, *4* (18), 6933–6939. https://doi.org/10.1039/c5ta08010j.

(52) Kämmerer, P. W.; Gabriel, M.; Al-Nawas, B.; Scholz, T.; Kirchmaier, C. M.; Klein, M. O. Early Implant Healing: Promotion of Platelet Activation and Cytokine Release by Topographical, Chemical and Biomimetical Titanium Surface Modifications in Vitro. *Clin Oral Implan Res* 2012, *23* (4), 504–510. https://doi.org/10.1111/j.1600-0501.2011.02153.x.

(53) Khosravi, N.; DaCosta, R. S.; Davies, J. E. New Insights into Spatio-Temporal Dynamics of Mesenchymal Progenitor Cell Ingress during Peri-Implant Wound Healing: Provided by Intravital Imaging. *Biomaterials* 2021, *273*, 120837. https://doi.org/10.1016/j.biomaterials.2021.120837.

(54) DiCecco, L.; D'Elia, A.; Miller, C.; Sask, K. N.; Soleymani, L.; Grandfield, K. Electron Microscopy Imaging Applications of Room Temperature Ionic Liquids in the Biological Field: A Review. *Chembiochem* 2021, *22* (15), 2488–2506. https://doi.org/10.1002/cbic.202100041.

(55) Lee, B. E. J.; DiCecco, L.; Exir, H.; Weck, A.; Sask, K. N.; Grandfield, K. Simultaneous Visualization of Wet Cells and Nanostructured Biomaterials in SEM Using Ionic Liquids. *Chembiochem* 2021, *22* (3), 571–576. https://doi.org/10.1002/cbic.202000552.

(56) Tsuda, T.; Mochizuki, E.; Kishida, S.; Iwasaki, K.; Tsunashima, K.; Kuwabata, S. SEM Observation of Hydrous Superabsorbent Polymer Pretreated with Room-Temperature Ionic Liquids. *Plos One* 2014, *9* (3), e91193. https://doi.org/10.1371/journal.pone.0091193.

(57) DiCecco, L.-A.; D'Elia, A.; Quenneville, C.; Soleymani, L.; Grandfield, K. Ionic Liquid Treatment for Efficient Sample Preparation of Hydrated Bone for Scanning Electron Microscopy. *Micron* 2021, 103192. https://doi.org/10.1016/j.micron.2021.103192.

(58) Huang, C.; Ness, V. P.; Yang, X.; Chen, H.; Luo, J.; Brown, E. B.; Zhang, X. Spatiotemporal Analyses of Osteogenesis and Angiogenesis via Intravital Imaging in Cranial Bone Defect Repair. *J Bone Miner Res* 2015, *30* (7), 1217–1230. https://doi.org/10.1002/jbmr.2460.

(59) Young, A.; McNaught, C.-E. The Physiology of Wound Healing. *Surg Oxf* 2011, *29* (10), 475–479. https://doi.org/10.1016/j.mpsur.2011.06.011.

(60) Kloxin, A. M.; Kloxin, C. J.; Bowman, C. N.; Anseth, K. S. Mechanical Properties of Cellularly Responsive Hydrogels and Their Experimental Determination. *Adv Mater* 2010, *22* (31), 3484–3494. https://doi.org/10.1002/adma.200904179.

(61) Mancini, M.; Moresi, M.; Rancini, R. Mechanical Properties of Alginate Gels: Empirical Characterisation. *J Food Eng* 1999, *39* (4), 369–378. https://doi.org/10.1016/s0260-8774(99)00022-9.

(62) Subramani, R.; Izquierdo-Alvarez, A.; Bhattacharya, P.; Meerts, M.; Moldenaers, P.; Ramon, H.; Oosterwyck, H. V. The Influence of Swelling on Elastic Properties of Polyacrylamide Hydrogels. *Frontiers Mater* 2020, *7*, 212. https://doi.org/10.3389/fmats.2020.00212.

(63) Papageorgiou, S. K.; Kouvelos, E. P.; Favvas, E. P.; Sapalidis, A. A.; Romanos, G. E.; Katsaros, F. K. Metal–Carboxylate Interactions in Metal–Alginate Complexes Studied with FTIR Spectroscopy. *Carbohyd Res* 2010, *345* (4), 469–473. https://doi.org/10.1016/j.carres.2009.12.010.

(64) Davis, T. A.; Volesky, B.; Mucci, A. A Review of the Biochemistry of Heavy Metal Biosorption by Brown Algae. *Water Res* 2003, *37* (18), 4311–4330. https://doi.org/10.1016/s0043-1354(03)00293-8.

(65) Farrokhpay, S.; Morris, G. E.; Fornasiero, D.; Self, P. Effects of Chemical Functional Groups on the Polymer Adsorption Behavior onto Titania Pigment Particles. *J Colloid Interf Sci* 2004, *274* (1), 33–40. https://doi.org/10.1016/j.jcis.2004.02.026.

(66) Socrates, G. *Infrared Characteristic Group Frequencies*; John Wiley & Sons, 2001.

(67) Redenski, I.; Guo, S.; Machour, M.; Szklanny, A.; Landau, S.; Kaplan, B.; Lock, R. I.; Gabet, Y.; Egozi, D.; Vunjak-Novakovic, G.; Levenberg, S. Engineered Vascularized Flaps, Composed of Polymeric Soft Tissue and Live Bone, Repair Complex Tibial Defects. *Adv Funct Mater* 2021, *31* (44), 2008687. https://doi.org/10.1002/adfm.202008687.

(68) Williams, R. T.; Bridges, J. W. Fluorescence of Solutions: A Review. *J Clin Pathol* 1964, *17* (4), 371. https://doi.org/10.1136/jcp.17.4.371.

(69) Zare, M.; Amin, M. M.; Nikaeen, M.; Bina, B.; Pourzamani, H.; Fatehizadeh, A.; Taheri, E. Resazurin Reduction Assay, a Useful Tool for Assessment of Heavy Metal Toxicity in Acidic Conditions. *Environ Monit Assess* 2015, *187* (5), 276. https://doi.org/10.1007/s10661-015-4392-y.

(70) Zhang, T.; Lin, S.; Shao, X.; Zhang, Q.; Xue, C.; Zhang, S.; Lin, Y.; Zhu, B.; Cai, X. Effect of Matrix Stiffness on Osteoblast Functionalization. *Cell Proliferat* 2017, *50* (3), e12338. https://doi.org/10.1111/cpr.12338.

(71) Golub, E. E.; Boesze-Battaglia, K. The Role of Alkaline Phosphatase in Mineralization. *Curr Opin Orthop* 2007, *18* (5), 444–448. https://doi.org/10.1097/bco.0b013e3282630851.

(72) Dondossola, E.; Friedl, P. Host Responses to Implants Revealed by Intravital Microscopy. *Nat Rev Mater* 2022, *7* (1), 6–22. https://doi.org/10.1038/s41578-021-00369-x.

(73) Greijer, A. E.; Wall, E. van der. The Role of Hypoxia Inducible Factor 1 (HIF-1) in Hypoxia Induced Apoptosis. *J Clin Pathol* 2004, *57* (10), 1009. https://doi.org/10.1136/jcp.2003.015032.

(74) Herbert, S. P.; Stainier, D. Y. R. Molecular Control of Endothelial Cell Behaviour during Blood Vessel Morphogenesis. *Nat Rev Mol Cell Bio* 2011, *12* (9), 551–564. https://doi.org/10.1038/nrm3176.

(75) Zan, T.; Du, Z.; Li, H.; Li, Q.; Gu, B. Cobalt Chloride Improves Angiogenic Potential of CD133+ Cells. *Front Biosci* 2012, *17* (7), 2247. https://doi.org/10.2741/4048.

(76) Jain, R. K. Molecular Regulation of Vessel Maturation. *Nat Med* 2003, *9* (6), 685–693. https://doi.org/10.1038/nm0603-685.

(77) Tung, J. J.; Tattersall, I. W.; Kitajewski, J. Tips, Stalks, Tubes: Notch-Mediated Cell Fate Determination and Mechanisms of Tubulogenesis during Angiogenesis. *Csh Perspect Med* 2012, *2* (2), a006601. https://doi.org/10.1101/cshperspect.a006601.

(78) Oakley, R.; Tharakan, B. Vascular Hyperpermeability and Aging. *Aging Dis* 2014, *5* (2), 114–125. https://doi.org/10.14336/ad.2014.0500114.

(79) Kumar, P.; Shen, Q.; Pivetti, C. D.; Lee, E. S.; Wu, M. H.; Yuan, S. Y. Molecular Mechanisms of Endothelial Hyperpermeability: Implications in Inflammation. *Expert Rev Mol Med* 2009, *11*, e19. https://doi.org/10.1017/s1462399409001112.

(80) Stratman, A. N.; Malotte, K. M.; Mahan, R. D.; Davis, M. J.; Davis, G. E. Pericyte Recruitment during Vasculogenic Tube Assembly Stimulates Endothelial Basement Membrane

Matrix Formation. *Blood* 2009, *114* (24), 5091–5101. https://doi.org/10.1182/blood-2009-05-222364.

(81) Chang, P.-C.; Seol, Y.-J.; Cirelli, J. A.; Pellegrini, G. R.; Jin, Q.; Franco, L. M.; Goldstein, S. A.; Chandler, L. A.; Sosnowski, B.; Giannobile, W. V. PDGF-B Gene Therapy Accelerates Bone Engineering and Oral Implant Osseointegration. *Gene Ther* 2010, *17* (1), 95–104. https://doi.org/10.1038/gt.2009.117.

(82) Caplan, A. I.; Correa, D. PDGF in Bone Formation and Regeneration: New Insights into a Novel Mechanism Involving MSCs. *J Orthopaed Res* 2011, *29* (12), 1795–1803. https://doi.org/10.1002/jor.21462.

(83) Sodek, J.; Chen, J.; NAGATA, T.; KASUGAI, S.; Todescan, R.; Li, I. W. S.; Kim, R. H. Regulation of Osteopontin Expression in Osteoblasts. *Ann Ny Acad Sci* 1995, *760* (1), 223–241. https://doi.org/10.1111/j.1749-6632.1995.tb44633.x.

(84) McKee, M. D.; Buss, D. J.; Reznikov, N. Mineral Tessellation in Bone and the Stenciling Principle for Extracellular Matrix Mineralization. *J Struct Biol* 2022, *214* (1), 107823. https://doi.org/10.1016/j.jsb.2021.107823.

(85) Kagiwada, H.; Yashiki, T.; Ohshima, A.; Tadokoro, M.; Nagaya, N.; Ohgushi, H. Human Mesenchymal Stem Cells as a Stable Source of VEGF-producing Cells. *J Tissue Eng Regen M* 2008, *2* (4), 184–189. https://doi.org/10.1002/term.79.

(86) Webb, N. J. A.; Bottomley, M. J.; Watson, C. J.; Brenchley, P. E. C. Vascular Endothelial Growth Factor (VEGF) Is Released from Platelets during Blood Clotting: Implications for Measurement of Circulating VEGF Levels in Clinical Disease. *Clin Sci* 1998, *94* (4), 395–404. https://doi.org/10.1042/cs0940395.

(87) Koehne, P.; Willam, C.; Strauss, E.; Schindler, R.; Eckardt, K.-U.; Bührer, C. Lack of Hypoxic Stimulation of VEGF Secretion from Neutrophils and Platelets. *Am J Physiol-heart C* 2000, *279* (2), H817–H824. https://doi.org/10.1152/ajpheart.2000.279.2.h817.

(88) Liao, D.; Johnson, R. S. Hypoxia: A Key Regulator of Angiogenesis in Cancer. *Cancer Metast Rev* 2007, *26* (2), 281–290. https://doi.org/10.1007/s10555-007-9066-y.

(89) Hirota, K.; Semenza, G. L. Regulation of Angiogenesis by Hypoxia-Inducible Factor 1. *Crit Rev Oncol Hemat* 2006, *59* (1), 15–26. https://doi.org/10.1016/j.critrevonc.2005.12.003.

(90) Pugh, C. W.; Ratcliffe, P. J. Regulation of Angiogenesis by Hypoxia: Role of the HIF System. *Nat Med* 2003, *9* (6), 677–684. https://doi.org/10.1038/nm0603-677.

(91) Kaur, B.; Khwaja, F. W.; Severson, E. A.; Matheny, S. L.; Brat, D. J.; Meir, E. G. V. Hypoxia and the Hypoxia-Inducible-Factor Pathway in Glioma Growth and Angiogenesis. *Neuro-oncology* 2005, *7* (2), 134–153. https://doi.org/10.1215/s1152851704001115.

(92) Li, Y.; Liu, Y.; Wang, C.; Xia, W.-R.; Zheng, J.-Y.; Yang, J.; Liu, B.; Liu, J.-Q.; Liu, L.-F. Succinate Induces Synovial Angiogenesis in Rheumatoid Arthritis through Metabolic Remodeling and HIF-1α/VEGF Axis. *Free Radical Bio Med* 2018, *126*, 1–14. https://doi.org/10.1016/j.freeradbiomed.2018.07.009.

(93) Sapieha, P.; Sirinyan, M.; Hamel, D.; Zaniolo, K.; Joyal, J.-S.; Cho, J.-H.; Honoré, J.-C.; Kermorvant-Duchemin, E.; Varma, D. R.; Tremblay, S.; Leduc, M.; Rihakova, L.; Hardy, P.; Klein, W. H.; Mu, X.; Mamer, O.; Lachapelle, P.; Polo, A. D.; Beauséjour, C.; Andelfinger, G.; Mitchell, G.; Sennlaub, F.; Chemtob, S. The Succinate Receptor GPR91 in Neurons Has a Major Role in Retinal Angiogenesis. *Nat Med* 2008, *14* (10), 1067–1076. https://doi.org/10.1038/nm.1873.

(94) DeCicco-Skinner, K. L.; Henry, G. H.; Cataisson, C.; Tabib, T.; Gwilliam, J. C.; Watson, N. J.; Bullwinkle, E. M.; Falkenburg, L.; O'Neill, R. C.; Morin, A.; Wiest, J. S. Endothelial Cell Tube Formation Assay for the In Vitro Study of Angiogenesis. *J Vis Exp* 2014, No. 91, e51312. https://doi.org/10.3791/51312.